Heliyon 10 (2024) e37890

Contents lists available at ScienceDirect

Heliyon

journal homepage: www.cell.com/heliyon

Research article

Abnormal intrinsic brain functional network dynamics in patients with retinal detachment based on graph theory and machine learning

Yuanyuan Wang [a,1], Yu Ji [b,1], Jie Liu [a], Lianjiang Lv [a], Zihe Xu [a], Meimei Yan [a], Jialu Chen [a], Zhijun Luo [a], Xianjun Zeng [a,*]

[a] Department of Radiology, The First Affiliated Hospital, Jiangxi Medical College, Nanchang University, Nanchang, China
[b] Department of Ophthalmology, The First Affiliated Hospital, Jiangxi Medical College, Nanchang University, Nanchang, China

ARTICLE INFO

Keywords:
Retinal detachment
Dynamic functional connectivity
Graph theory analysis
Brain functional network
Machine learning

ABSTRACT

Background: and purpose: The investigation of functional plasticity and remodeling of the brain in patients with retinal detachment (RD) has gained increasing attention and validation. However, the precise alterations in the topological configuration of dynamic functional networks are still not fully understood. This study aimed to investigate the topological structure of dynamic brain functional networks in RD patients.

Methods: We recruited 32 patients with RD and 33 healthy controls (HCs) to participate in resting-state fMRI. Employing the sliding time window analysis and K-means clustering method, we sought to identify dynamic functional connectivity (dFC) variability patterns in both groups. The investigation into the topological structure of whole-brain functional networks utilized a graph theoretical approach. Furthermore, we employed machine learning analysis, selecting altered topological properties as classification features to distinguish RD patients from HCs.

Results: All participants exhibited four distinct states of dynamic functional connectivity. Compared to the healthy control (HC) group, patients with RD experienced a significant reduction in the number of transitions among these four states. Additionally, the dynamic topological properties of RD patients demonstrated notable changes in both global and node-specific characteristics, with these changes correlating with clinical parameters. The support vector machine (SVM) model used for classification achieved an accuracy of 0.938, an area under the curve (AUC) of 0.988, and both sensitivity and specificity of 0.937.

Conclusion: The alterations in the topological properties of the brain in RD patients may indicate the integration function and information exchange efficiency of the whole brain network were reduced. In addition, the topological properties hold considerable promise for distinguishing between RD and HCs.

1. Introduction

Retinal detachment (RD) occurs due to the separation of the retinal nerve epithelium and pigment epithelium, which is a prevalent

* Corresponding author.
E-mail address: xianjun-zeng@126.com (X. Zeng).
[1] Equal contribution authors.

https://doi.org/10.1016/j.heliyon.2024.e37890
Received 13 July 2024; Received in revised form 10 September 2024; Accepted 12 September 2024
Available online 2 November 2024

and severe ocular disorder leading to vision loss. Several forms of RD exist, with rhegmatogenous being the most common among them [1]. Research suggests that the worldwide yearly occurrence of RD is approximated at 12.17 instances per 100,000 individuals, with Europe exhibiting the highest incidence, followed by the Western Pacific region and the Americas among the world's geographic areas. There is evidence pointing towards a rising trend in the incidence of RD over time, potentially resulting in a doubling of the current rate within the next two decades [2]. In the initial stages of RD, patients typically manifest symptoms such as acute floaters, flashing lights, and visual field defects. As the lesion extends into the macular area, it results in vision loss, potentially progressing to blindness. Some patients may experience anxiety, depression, or cognitive impairment, which brings a heavy burden to society and families [3,4].

Various risk factors are linked to the prevalence of RD, encompassing retinal tears, high myopia, previous cataract surgery, and a familial history of RD [5]. These risk factors can induce retinal or vitreous degeneration, leading to the accumulation of fluid under the neurosensory retina, which is a critical characteristic of RD. Prior research has demonstrated that vision impairment in patients with RD primarily results from the depletion of photoreceptor cells [6]. In a clinical context, the photoreceptor cells persist in undergoing apoptosis for a duration even after the successful surgical repair of RD [7]. Photoreceptor cells are situated in the retinal neuroepithelium, which is considered extensions of the central nervous system (CNS). This implies the potential presence of CNS abnormalities in patients with RD [8]. Presently, there exist three types of in vivo and in vitro models for studying the pathophysiological mechanisms of retinal detachment. However, each model possesses both advantages and disadvantages, so the pathogenesis of retinal detachment is still unclear [9,10].

At present, the diagnosis of RD predominantly depends on clinical ophthalmological examinations, including optical coherence tomography (OCT), ocular B-scan, fundus microscopy, and slit-lamp microscopy. These examinations aid in identifying the type of RD and extent of detachment [11]. However, these tests solely examine ocular function and cannot evaluate potential abnormalities in the CNS of patients with RD. As a non-invasive imaging method, rs-fMRI has gained growing popularity for studying the intrinsic activity of the brain, which provide a new direction for the pathophysiological mechanism of RD [12–14]. Retinal detachment, as a serious eye disease, can lead to impaired visual information processing, and this sensory loss or change may trigger adjustment or reorganization of the brain in visual processing and related functional networks. Several recent studies have demonstrated that patients with RD exhibit abnormal functional connection density [15] and percent amplitude of fluctuation [16] in vision-related brain regions. Moreover, Ji et al. found that dALFF, functioning as a local indicator of brain activity, could be valuable in clinical diagnosis [17]. Currently, there is a scarcity of fMRI studies on patients of RD both domestically and internationally. Most investigations have predominantly concentrated on the local brain regions or individual indices of RD. Nevertheless, the alterations in global brain functional networks among patients with RD remain inadequately understood.

Brain networks can be classified into regular networks, random networks, and "small-world" networks [18]. In regular network, the Lp is longer, and Cp is higher. Conversely, random network exhibits a shorter Lp and a lower Cp. Graph theory has become increasingly prominent for illustrating the intricate network maps of the human brain, both structurally and functionally [19]. This approach reveals how the brain operates as a sophisticated and interconnected network. Graph theory has found application in the investigation of Alzheimer's disease (AD) [20,21], schizophrenia [22] and cervical spondylotic myelopathy (CSM) [23,24]. Liu et al. employed graph theory to investigate changes in functional connectivity among primary angle-closure glaucoma (PACG) patients. Their findings indicate that PACG patients sustain the stability of brain networks through compensatory effects in both visual and non-visual areas [25]. It is of significance to investigate whether RD as an ophthalmic disease has similar topological characteristics to PACG patients. Since similar topological characteristics may reveal the similarities in brain function between these two eye diseases, it provides a new perspective for understanding the pathogenesis of RD. To enhance the observation of temporal changes in brain functional activity among patients with RD, we integrated graph theory analysis with sliding time window analysis. Utilizing the K-means clustering method, the outcomes within each sliding time window can be partitioned into distinct states, enhancing the description of the working patterns of the human brain throughout the scanning process. Finally, different machine learning models were constructed to distinguish between patients with RD and healthy people. Machine learning models are able to learn and recognize disease patterns from large amounts of data, thereby improving the accuracy of diagnosis. This is one of the hot spots in current research and has been applied to many diseases [26,27].

The aim of this study was to capture the dynamic configurations of brain networks in patients with RD. We hypothesized that (i) patients with RD showed a different dynamic connectomic pattern than HCs; (ii) the topological attributes of RD patients showed temporal variability; (iii) topology attribute values serve as sensitive biomarkers capable of distinguishing patients with RD from HCs.

2. Materials and methods

2.1. Participants

This study employed an observational case-control design, with sample size calculation based on a two-sample approach to test differences between patients with RD and HCs. The power calculation was conducted using the G-Power3.1 software (http://www.gpower.hhu.de/).This study comprised 32 RD patients diagnosed by the First Affiliated Hospital of Nanchang University from January 2023 to September 2023, along with 33 HCs carefully matched for age, sex, and education level. The selection criteria for patients with RD were as follows: (1) idiopathic RD impacting one or both retinal tears, (2) RD involving up to two quadrants, and (3) no concurrent eye conditions in either eye. Conversely, patients were excluded if they had (1) recurring RD, (2) RD linked to high myopia, (3) RD caused by ocular trauma, (4) RD with severe complications, (5) a history of surgical procedures, (6) cardiovascular disease, and (7) mental health disorders or cerebral infarction.

Inclusion criteria for the HC group included the absence of eye diseases and major illnesses (such as cerebral infarction) and

uncorrected visual acuity greater than 1.0. All participants underwent magnetic resonance imaging and relevant pertinent eye examinations. The intraocular pressure was measured using an tonometer. The Hamilton Anxiety (HAMA) and Hamilton Depression (HAMD) Scales were used to assess whether patients with RD had anxiety and depression. And the Montreal Cognitive (MoCA) Scale was used to assess cognitive function in patients with RD. We calculate the score by asking questions on the scale. These scales have been validated to provide consistent and reliable assessment criteria, making results more comparable.

2.2. MRI data acquisition

All participants were scanned using a 3.0 T MRI system (Siemens Trio Tim, Erlangen, Germany) equipped with an 8-channel phased array head coil, located at the Department of Radiology, The First Affiliated Hospital, Jiangxi Medical College, Nanchang University. Table 1 details the specific scanning parameters.

2.3. Data pre-processing

Rs-fMRI data processing was conducted using the DPABI toolbox v6.0 [28]. The preprocessing involved several steps: (1) conversion of image formats and exclusion of the initial ten time points; (2) correction for temporal levels and head movements; (3) alignment of functional data with T1-weighted structural images; (4) standardizing image dimensions to Montreal Neurological Institute (MNI) space and resampling to a $3 \times 3 \times 3$ mm^3 voxel size; (5) elimination of linear drift and covariates; (6) global signal regression, including white matter and cerebrospinal fluid; and(7) applying a bandpass filter within the 0.01–0.08 Hz frequency range.

2.4. Construction of dynamic functional networks

The dynamic functional connectivity (dFC) matrix for each participant was created using the DynamicBC analysis toolbox [29], employing a sliding time window technique. This method involved a 30 TR window length and a 1 TR step size. According to previous studies, spontaneous activities can be better captured within 30–60s of window length, and different window lengths within this range have little impact on the results [30]. Then we get 201 Windows, each scanned 30 times. The brain's 90 anatomical regions were delineated using the Automatic Anatomical Labeling 90 (AAL) atlas. For each window, we calculated the Pearson correlation coefficient across all brain region time series, resulting in a 90x90 matrix per window for each subject. We performed fisher Z transformation on all the matrices to bring the data closer to the normal distribution. We then assessed the Z-values to depict temporal fluctuations in the correlation coefficient, which effectively represented the variability in dFC.

2.5. Characteristics of dynamic functional networks

K-means clustering was then applied to classify the functional connectivity matrix. This analysis used city block distances to measure the similarity between different time windows. The optimal number of clusters was determined using the elbow criterion, a widely used method known for its intuitiveness, simplicity, and clarity [31]. The range of variation of k was 2–10, and the optimal number of clusters $k = 4$ .The dFC matrix of all subjects was clustered into four dFC states, which were recurrent instantaneous FC patterns across different windows and subjects. A state was considered effective when it contains at least 10 windows. From the FC time series, we extracted data to quantify several temporal characteristics: (1) the fraction of time, denoting the percentage of each state within the four states, (2) mean dwell time, representing the average time a subject spent in a specific state, and (3) transition number, indicating the frequency with which a subject transitioned between states.

We then extracted the variability matrix for all subjects and the brain networks in each state. The two-sample *t*-test was further used to compare differences between groups (with age, gender, and education as covariates; network-based statistics correction with edge p \0.001, component p\ 0.05, literation = 1000).

Table 1
Scan parameters for all sequences.

Parameters	3D-T1	EPI
TR(ms)	1900	2000
TE (ms)	2.26	30
flip angle	9°	90°
FOV(mm^2)	256 × 256	200 × 200
matrix	256 × 256	64 × 64
slice thickness(mm)	1	4
number of slices	176	30
voxel size(mm^3)	1.0 × 1.0 × 1.0	3.0 × 3.0 × 4.0
interslice gap(mm)	0.5	1.2
number of scans	256	240
duration	3 min and 34 s	8 min and 6 s

TR, repetition time; TE, echo time; FOV: field of View; EPI, echo-planar imaging.

2.6. Graph theory analysis of dynamic functional networks

The dFC networks, derived from all sliding time windows, underwent an evaluation of their topological characteristics using graph theory-based methods [32]. The global properties are as follows: (1) global efficiency, quantifies how efficiently information is exchanged across the entire network; (2) local efficiency, refers to the average of the local efficiency of the entire network; (3) small world, characterizes networks that exhibit both high clustering and short average path lengths. When calculating small-world properties, the number of randomizations for random networks is 1000. The parameters measured are as follows: (a) characteristic path length (Lp): the average shortest path length between any pairs of nodes; (b) clustering coefficient (C_p):the average inter-connectedness of a node's direct neighbors; (c) normalized clustering coefficient(γ): the clustering coefficient compared to matched random networks; (d) normalized characteristic path length(λ): the characteristic shortest path length compared to matched random networks; (e) small-worldness (σ):the normalized clustering coefficient divided by the normalized characteristic shortest path length, which reflect the balance of global efficiency and local efficiency. The nodal properties are as follows: (1) nodal degree centrality, measures the number of connections a node has in the network; (2) nodal betweenness centrality, quantifies the extent to which a node lies on the shortest paths between other pairs of nodes in the network; (3) nodal local efficiency, refers to the efficiency of information transmission on the direct neighbors of a node; (4) nodal clustering coefficient, measures the degree to which its neighbors are interconnected. The mathematical equations of all topological properties have been described in previous studies [33]. This analysis was conducted with the GRETNA toolkit v2.0.0 [34]. To mitigate the impact of spurious relationships on interregional connectivity, we established the network sparsity range from 0.1 to 0.4, using intervals of 0.01 as suggested by prior research [35]. At this sparsity, all subjects' networks have small-world properties (sigma$>$1.1). We assessed the variability of both global and nodal network metrics within each dFC network and sliding time window. When calculating gamma and lambda values, the Watts-Strogatz model of small-world networks was used as a benchmark to evaluate whether the topology of the network was significant [18]. In addition, we used the null model proposed by Maslov and Sneppen as a control group to better evaluate the characteristics of the actually observed network [36]. A two-sample T-test was then applied to determine the temporal fluctuations in these metrics, illuminating the evolving topological dynamics of the brain networks.

2.7. Statistical analysis

For statistical analysis, we used SPSS software v26.0.[2] Continuous variables' group differences were analyzed using a two-sample *t*-test, whereas categorical variable disparities were examined using the Chi-square test. For the comparison of dynamic topological attributes between the two groups, FDR correction was used to reduce the incidence of a class of errors, and $q < 0.05$ was considered to be statistically significant. Subsequently, we explored the relationship between dynamic functional network metrics and clinically relevant parameters, as well as scale scores within the RD group.

2.8. Machine learning analysis

To assess the diagnostic potential of dynamic graph theory attributes for RD, we use machine learning to classify them. There were many options for the input of the model, and we ultimately chose a support vector machine (SVM) model for classification. SVM is a supervised learning model suitable for classification and regression tasks with small sample sizes. SVM performs classification by maximizing the margin between classes. Key parameters include the penalty parameter C, the kernel function parameter γ, the type of kernel function, and class weights. Adjusting these parameters can optimize model performance, typically achieved through cross-validation to select the best parameter combination [37]. The procedural steps include: (1) extracting variation values of all dynamic brain network graph theory attributes; (2) select the appropriate kernel function and set parameters, train the SVM model, and optimize the parameters by leaving a cross-validation; (3) model evaluation and prediction.

3. Results

3.1. Demographics and clinical characteristics

There was no significant difference in age ($P = 0.868$), sex ($P = 0.806$) and education level ($P = 0.115$) between RD patients and HCses of RD patients are shown in Table 2.

3.2. Temporal characteristics of dynamic functional networks

Applying the elbow rule determined the optimal cluster number K as 4. In these clusters, we discerned four distinct states in the subjects' resting state MRI scans: status 1(34.06 %), status 2(15.54 %), status 3(32.84 %), and status 4(17.56 %) (Fig. 1). The RD group demonstrated fewer transitions between these states compared to the HC group. Furthermore, no notable differences were found in frequency and MDT for both groups, as shown in Fig. 2.

[2] https://www.ibm.com/support/pages/downloading-ibm-spss-statistics-26.

Table 2
Demographic and clinical characteristics of the subjects.

Condition	RD(n = 32)	HC(n = 33)	P-value
Age(years)	53.22 ± 18.57	52.55 ± 13.73	0.868
Gender(male/female)	17/15	17/16	0.806
Education(years)	9(9, 12)	9(8.5, 10.5)	0.115
Disease duration(days)	17.5(7, 30)	N/A	N/A
IOP (mmHg)	14.08 ± 3.47	N/A	N/A
Axial length of eye(mm)	24.44 ± 1.62	N/A	N/A
Corneal endothelial cell count (mm2)	2366.7 ± 472.65	N/A	N/A
HAMA	3(1.25, 4.75)	N/A	N/A
HAMD	3(1, 4)	N/A	N/A
MoCA	19.94 ± 6.24	N/A	N/A

RD, retinal detachment; HC, healthy control; IOP, intraocular pressure; HAMA, Hamilton Anxiety Scale; HAMD, Hamilton Depression Scale; MoCA, Montreal Cognitive Assessment; N/A, not applicable.

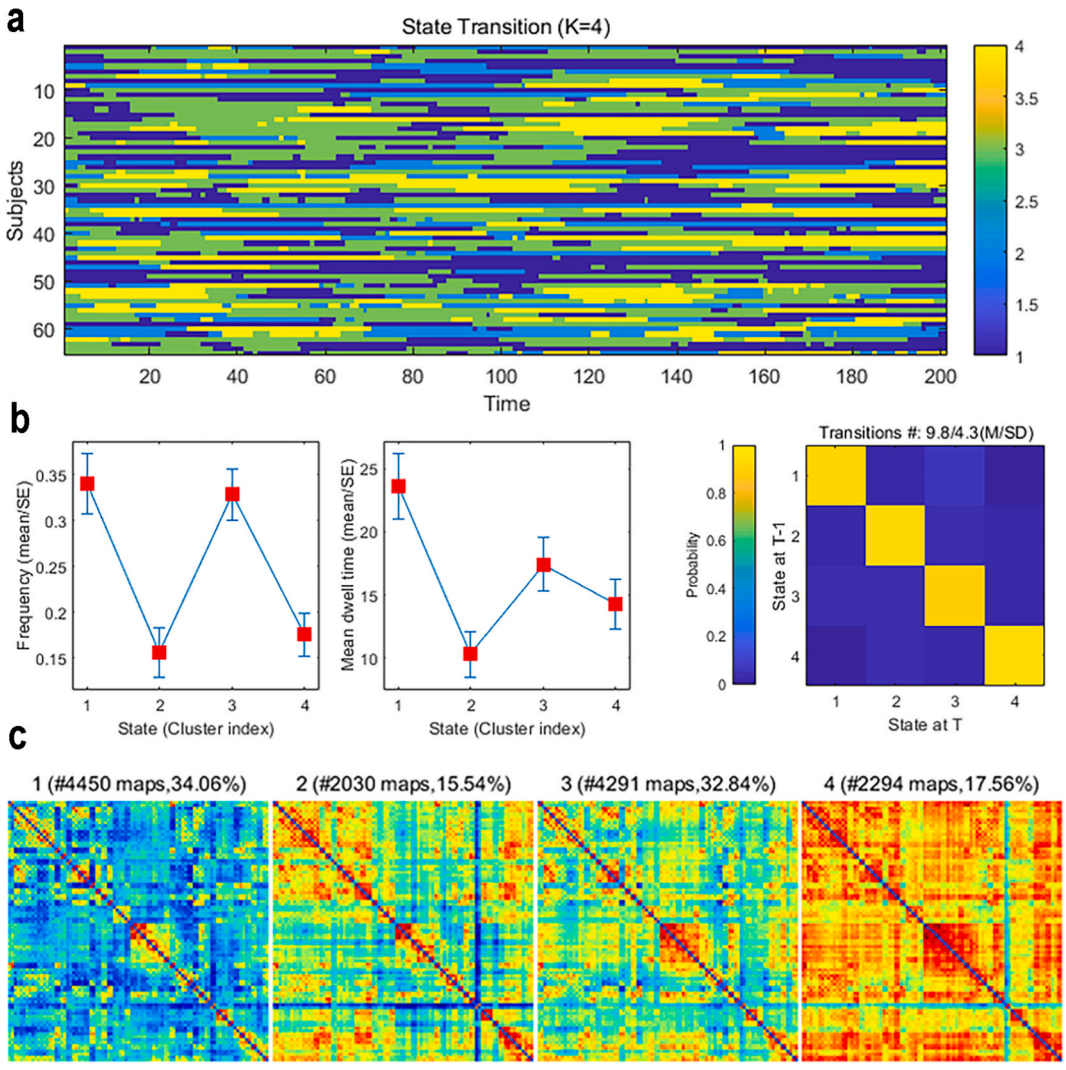

Fig. 1. The state-switching pattern across all subjects and sliding windows; It also shows the transition numbers (a) and MDT(b) among state 1, state 2, state 3, and state 4, as well as the occurrence frequencies of these states(c).

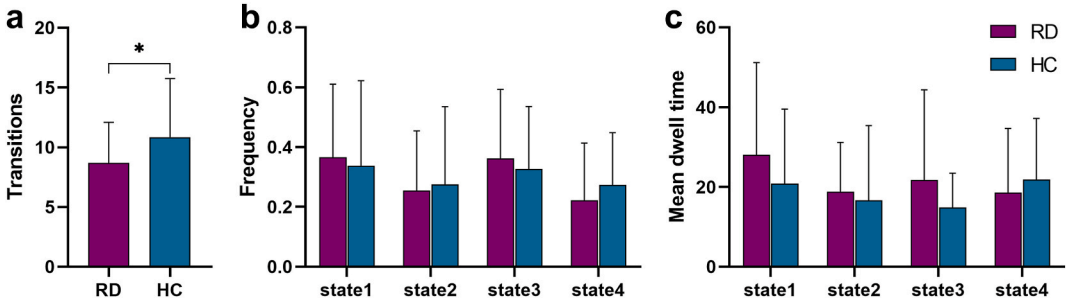

Fig. 2. Differences of temporal properties between the two groups. A significant variance was found in the number of transitions (mean ± SD for RD patients: 8.45 ± 3.61; for healthy controls: 10.59 ± 5.06, $p < 0.05$). but not in MDT or state frequency. The RD and HC groups are represented by purple and blue, respectively.

3.3. Differences in edge analysis between RD and HC groups

All brain regions were classified into corresponding networks according to the RSN map. There were no significant differences in functional brain connectivity between the two groups in the four states. However, compared with HC, the variation values was significantly reduced in the RD group. It was mainly manifested in Auditory Network (AN) and Salience Network (SN), AN and Default Mode Network (DMN), AN and Visual Network (VN) (Fig. 3).

3.4. Dynamic topological properties of brain networks

We found that compared with HC, RD patients had a small-world attribute, and the variance of L_p ($p < 0.001$), C_p ($p < 0.001$), γ($p < 0.001$), λ ($p = 0.002$) andσ($p < 0.001$) were significantly reduced, while no difference was found between global efficiency(E_{glob}) and local efficiency(E_{loc}) (Fig. 4).Moreover, significant variations were observed in node attributes, including measures such as degree centrality, nodal efficiency, betweenness centrality, nodal cluster coefficient, predominantly within networks like the auditory (AN), salience (SN), precuneus (PN), executive control (ECN), sensorimotor (SMN), default mode (DMN), and visual (VN), detailed in Table 3 and Fig. 5. All data were corrected by the Bonferroni correction, with a significance threshold set at $p < 0.05$.

3.5. Relationships between network properties and clinical variables

The dynamic graph theory attributes of RD patients were significantly correlated with the disease duration, corneal endothelial cell count and MoCA scores. However, no significant correlations were found among the three dynamic time features (NT, Frequency, MDT) in patients with RD (Fig. 6).

3.6. Machine learning results

After synthesizing the classification efficiency of all models, we found that SVM model has a better classification effect on small samples. The classification accuracy of SVM model is 0.938, the area under the curve (AUC) is 0.988, the sensitivity is 0.937, and the specificity is 0.937. The AUC is shown in Fig. 7.

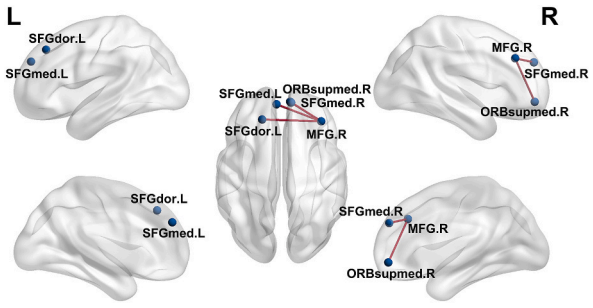

Fig. 3. The result of the variability connection matrix. SFGdor, superior frontal gyrus, dorsolateral; SFGmed, superior frontal gyrus, medial; ORBsupmed, superior frontal gyrus, medial orbital; MFG, middle frontal gyrus; L, left; R, right.

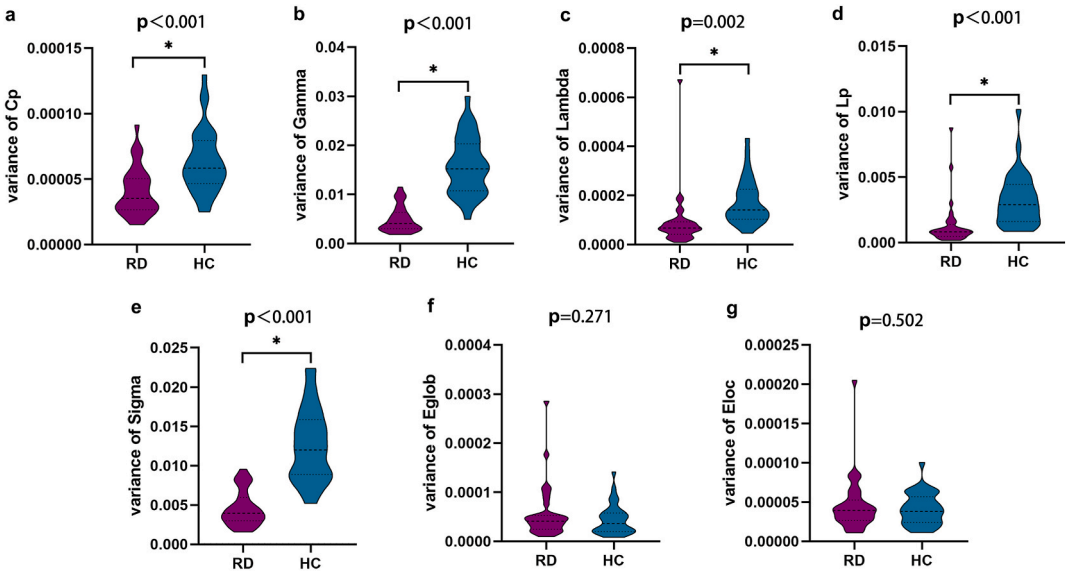

Fig. 4. Between-group comparisons of; (a) clustering coefficient (Cp), (b) normalized clustering coefficient (γ), (c) normalized characteristic path length (λ), (d) characteristic path length (Lp), (e) small-worldness (σ), (f) global efficiency (Eglob), and (g) local efficiency (Eloc). *Bonferroni p < 0.05.

Table 3
Abnormal topological properties in RD and HCs groups.

Brain networks	Brain regions	FDR q values			
		Nodal degree	Nodal efficiency	Nodal betweenness	Nodal cluster coefficient
Auditory network	ORBmid.L	0.676	0.96	**0.032**	0.864
	ORBmid.R	0.679	0.402	**0.02**	0.637
Salience network	ORBsup.L	**0.006**	0.496	0.983	0.519
	CUN.R	0.653	0.736	**0.02**	0.881
Precuneus network	MOG.R	0.716	**0.049**	0.57	**0.028**
Executive control network	HIP.R	**0.011**	0.278	0.192	0.603
	PHG.L	0.979	**0.038**	0.972	**0.017**
	SPG.L	**0.027**	0.274	0.348	0.662
	SMG.L	0.089	0.06	0.1	**0.042**
Sensorimotor network	SMG.R	0.799	0.26	0.078	**0.036**
	ANG.L	0.481	0.296	0.782	**0.049**
	ANG.R	**0.023**	**0.015**	0.131	**0.026**
Default mode network	CAU.L	**0.031**	0.144	0.721	**0.003**
Visual network	STG.L	0.634	0.111	0.678	**0.025**
	STG.R	0.234	0.056	0.108	**0.033**
	TPOsup.L	**0.005**	**0.001**	0.812	**0.003**
	TPOmid.L	0.558	0.162	**0.031**	0.059
	TPOmid.R	**0.027**	0.101	0.233	0.182
	ITG.L	0.059	0.106	0.233	**0.047**
	ITG.R	0.948	0.277	0.969	**0.026**

Marking regions as abnormal if they showed significant inter-group disparities (FDR q < 0.05). RD, retinal detachment; HCs, healthy controls; ORBmid, middle frontal gyrus, orbital part; ORBsup, superior frontal gyrus, orbital part; CUN, cuneus; MOG, middle occipital gyrus; HIP, hippocampus; PHG, parahippocampal gyrus; SPG, superior parietal gyrus; SMG, supramarginal gyrus; ANG, angular gyrus; CAU, caudate nucleus; STG, superior temporal gyrus; TPOsup, temporal pole: superior temporal gyrus; TPOmid, temporal pole: middle temporal gyrus; ITG, inferior temporal gyrus; L, left; R, right.

4. Discussion

The purpose of this study was to investigate the temporal characteristics of dynamic brain networks and the variability of network topological organization in patients with RD. Through clustering analysis and graph theory analysis, we reveal significant differences between the two groups and explore the mechanisms by which these differences may be related to RD.

We delineated four distinct states through the clustering of topography network maps derived from subjects across all sliding time windows. Commonly, parameters such as NT, MDT, and frequency are employed in dynamic pattern analysis to depict state properties

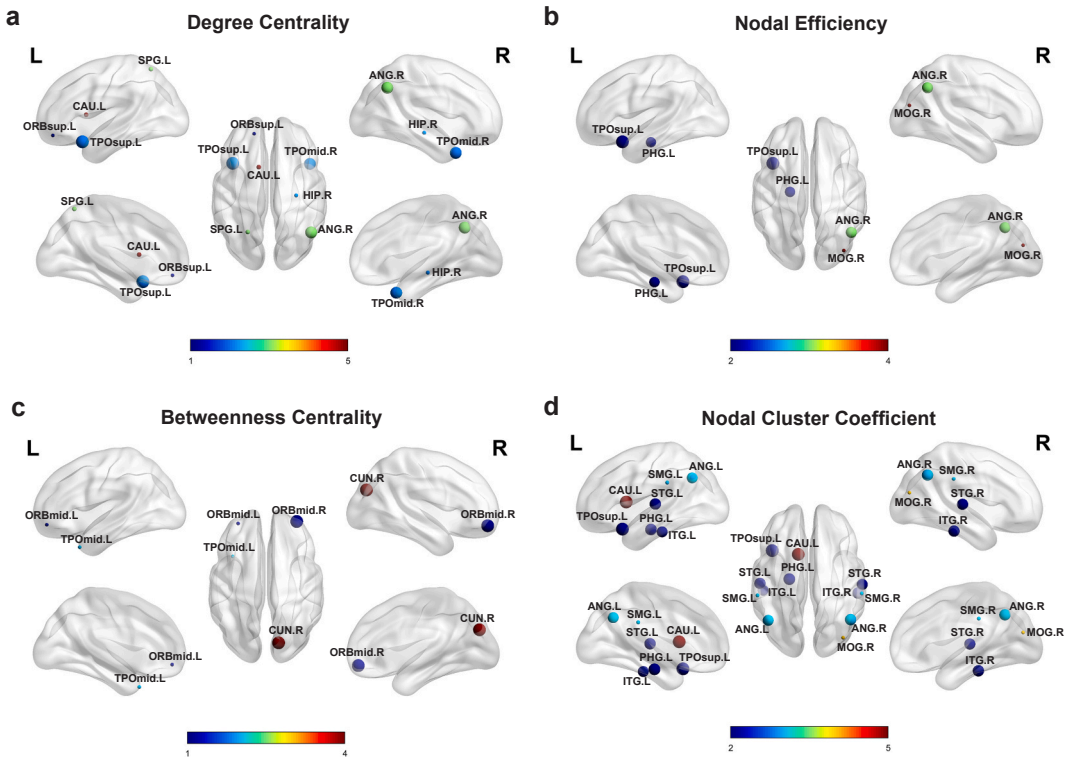

Fig. 5. Compares degree centrality(a), nodal efficiency(b), betweenness centrality(c), and nodal cluster coefficient(d) between groups. Color bars represent t-scores; warm colors indicate areas of increased node variance in RD patients and cooler colors showing the converse.

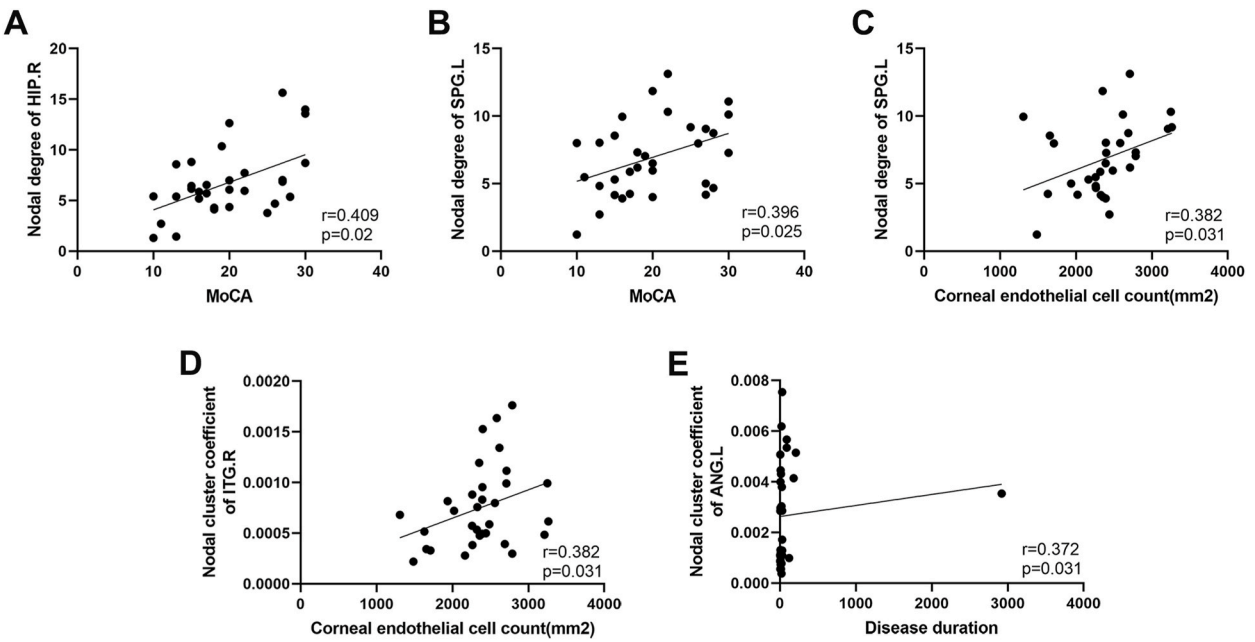

Fig. 6. Correlation analysis results between variance values of topological attributes of nodes and clinical parameters. HIP, hippocampus; SPG, superior parietal gyrus; ITG, inferior temporal gyrus; ANG, angular gyrus; L, left; R, right.

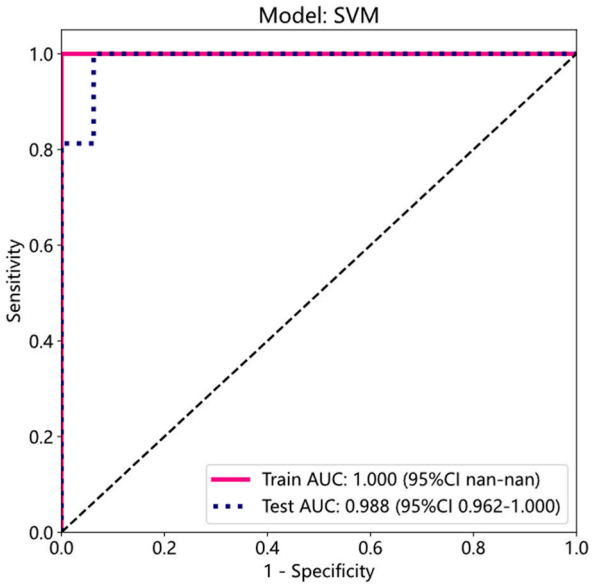

Fig. 7. AUC diagram of SVM model. The red line represents the training set, and the purple dashed line represents the test set.

[38]. These properties capture brain functional activity and have the potential to undergo reconfiguration during illness [39]. In the present study, the RD group exhibited a greater NT between the four states compared to the HC group. These differences in NT may reflect the spontaneous characteristics of patients with RD. Previous research has demonstrated a correlation between the augmentation of NT and a reduction in information flow efficiency within the brain network [40]. RD is known to affect the normal function of the retina, resulting in abnormalities in image processing and perception, which is consistent with the pattern of high NT we found. These results support the theory of neurological and perceptual dysfunction caused by RD, suggesting that NT may be a valuable indicator for assessing RD. In addition, the variation values of RD group was significantly reduced compared with HC group. It is mainly manifested in AN and SN, AN and DMN, AN and VN. This finding suggests that AN is the main damaged network, which is consistent with previous findings in glaucoma, suggesting that the two may have similar pathogenesis [41].

Small-world networks have been observed in many diseases and are thought to be a favorable balance of local brain specialization and global integration, characterized by longer Cp and shorter Lp [42–44]. In this study, the variance of all small-world attributes (Cp, Lp, γ, λ, σ) in patients with RD were lower than HCs. These findings indicate that the brains of patients with RD exhibit a tendency to be "fragile" and prone to disturbances and damage. Cp may be linked to diminished functional connectivity in specific brain regions due to pronounced demyelination, which also observed in optic neuritis [45]. Lp gauges the capacity for information transmission across the network and is associated with cognitive function [46]. The parameter γ, serving as a standardized clustering coefficient, assesses network dispersion, with lower values indicative of reduced grouping. In patients with RD, optic nerve impairment may result in damage to the pertinent brain hemispheres, potentially altering brain function area values and leading to cognitive dysfunction. Nevertheless, diminished values of λ and σ signify a reduction in local specialization among RD patients, suggesting a propensity for the transformation of the brain functional network towards a random network. This network randomization has also been observed in cases of PACG and CSM [23,25]. Furthermore, an investigation centered on patients with drug-naive social anxiety disorder (SAD) revealed a reduced λ in SAD, which suggests a transition towards a random configuration in the network topology characteristic of SAD patients [47]. Compared with small-world networks, random networks have lower modularity and fault tolerance in information processing [48]. The observed randomization in RD patients suggests a less optimal organization of their brain's functional networks, hinting at potential dysfunction in brain network integration for individuals with RD. Various research indicates that dynamic variability in brain networks might boost information integration and augment cognitive process flexibility [49,50]. Nonetheless, RD patients exhibited no notable differences in the variance of global and local efficiency. This may be a structural adaptation to compensate for the brain integration dysfunction in RD patients and maintain the overall brain information transmission efficiency.

Additionally, RD and HC displayed notable distinctions in the variability of node attributes. For degree centrality, significant differences were mainly concentrated in SN, ECN, SMN, DMN and VN. Degree centrality quantifies the number or sum of weights of connections directly linked to a node [51]. A study on RD has indicated a close association between the visual function changes in RD patients and the functional connections of the DMN [13]. DMN and ECN fulfill roles in cognitive control and emotional regulation. Specifically, DMN facilitates internal psychological exploration, while ECN is involved in processing external stimuli and tasks. And SN plays a crucial role in detecting conflicts between these two networks and maintaining a balance in the transition between introverted and extroverted cognitive states [52,53]. Therefore, we speculated that the decreased variance of degree centrality of DMN, ECN and SN might be caused by the decline of cognitive function in patients with RD. Furthermore, earlier research has indicated a close relationship between the SMN and the spontaneous brain activity linked to the primary visual cortex [54], and the intimate correlation between these two elements holds significant importance in the processing of spatial visual information [55]. This suggest that SMN

and VN have synergistic functions. Owing to the damage to photoreceptor cells in patients with RD, there is a reduction in visual information input, leading to compensatory increases in the functional activities of SMN and VN. Interestingly, brain regions with significant differences in node efficiency and nodal cluster coefficient were distributed within similar networks. Node efficiency reflects the effectiveness of information transfer among a node's immediate neighbors, while the nodal cluster coefficient denotes the inter-connectedness of those direct neighbors [51]. It is noteworthy that both the node efficiency and nodal cluster coefficient of PN exhibit a reduction. Previous investigations have underscored the significant role of the precuneus in DMN [56]. Wu et al. [57] have reported that PN might be implicated in the compensatory mechanism of Type 2 Diabetes Mellitus-Related Cognitive Impairment (T2DM-NCI), highlighting the precuneus as a potentially sensitive neuroimaging feature indicative of cognitive impairment. This aligns with the previous results, indicating that the dynamic changes of PN may predict cognitive changes in patients with RD. Betweenness centrality signifies a node's impact on directing information flow among other nodes [51]. In this study, we found that the variance of betweenness centrality in AN both increased and decreased, indicating that the information flow in the auditory network was unstable, or it might be the result of remodeling in the network. Furthermore, betweenness centrality of VN, pivotal in visual information processing, exhibited a reduction. The interaction between VN and AN may reveal sensory information integration disorders. Shu et al. [58] postulated a plausible hypothesis in their research, suggesting that diminished interhemispheric information processing within VN among Primary Angle-Closure Glaucoma (PACG) patients might induce alterations in the capacity of SN to receive external stimuli. Therefore, we speculate that the impairment of VN in patients with RD could potentially result in an augmentation of the compensatory function of SN. These networks are both independent and interconnected. This indicates that RD is not a single network damage disease, but spans multiple networks.

Correlation analysis showed that the small-world attribute and nodal attribute of RD patients were significantly correlated with clinical ophthalmology parameters and scale scores. The node efficiency within ECN demonstrated a positive correlation with both MoCA scores and corneal endothelial cell counts. Likewise, there was a positive correlation between the nodal cluster coefficient within VN and corneal endothelial cell count. Endothelial cells play a crucial role in maintaining the function and transparency of the cornea. As individuals age, corneal endothelial cell counts naturally decrease. However, dysfunction in these cells can also contribute to a reduction in corneal endothelial cells [59]. This suggests that as disease advances and cognitive function declines in RD patients, the information transmission efficiency of nodes in ECN and VN will be affected. Furthermore, the nodal cluster coefficient of SN showed a negative correlation with the disease duration. This suggests that the brain network changes may occur in the early stage of RD.

In this study, SVM model was used to classify RD patients based on dynamic graph theory attributes. The classification accuracy of SVM model is 0.938, the area under the curve is 0.988, the sensitivity is 0.937, and the specificity is 0.937. Therefore, we speculate that dynamic graph theory properties can be used as sensitive biomarkers to distinguish patients with RD and HCs. Of course, these results need to be verified by large samples and multi-center experiments.

4.1. Limitation

Several limitations exist. Primarily, this cross-sectional study elucidates the dynamic connectivity patterns in the brain networks of RD patients, necessitating longitudinal studies to gauge surgical impacts on changes within this dynamic connectome. Additionally, the inclusion of all RD patients might obscure distinctions among varying patient types in dynamic brain network results. Moreover, this study solely scrutinized disparities in functional brain networks among RD patients, warranting further exploration into the topological attributes of structural brain networks. Finally, the count of data set in this study is too less for using a high standard machine learning algorithm, and larger data sets will be needed to validate this result in the future.

5. Conclusion

In our research, we employed sliding time window techniques along with graph theory approaches to analyze alterations in the dynamic structure of whole-brain functional networks among RD patients. We found that the variance of small-world attribute was generally reduced in RD patients, indicating that the integration function of whole brain network and the efficiency of information exchange were reduced in RD patients. In addition, there were significant differences in the variance of node attributes in patients with RD, mainly concentrated in SN, ECN, SMN, DMN, VN, AN and PN. This provided imaging evidence to explain cognitive impairment in patients with RD. This study not only pinpointed irregularities in these networks, but it also enhanced existing knowledge regarding resting brain networks in RD patients. In addition, we usedmachine learning models to classify patients with RD and found that dynamic graph theory attributes might offer sensitive markers to differentiate RD patients from HCs.

CRediT authorship contribution statement

Yuanyuan Wang: Writing – review & editing, Writing – original draft, Methodology, Formal analysis, Conceptualization. **Yu Ji:** Writing – review & editing, Methodology, Conceptualization. **Jie Liu:** Methodology, Formal analysis. **Lianjiang Lv:** Visualization, Software. **Zihe Xu:** Software, Data curation. **Meimei Yan:** Data curation. **Jialu Chen:** Data curation. **Zhijun Luo:** Data curation. **Xianjun Zeng:** Writing – review & editing, Validation, Supervision, Project administration.

Ethics and consent statement

This study received approval from the Human Research Ethics Committee of the First Affiliated Hospital of Nanchang University and adhered to the principles outlined in the Declaration of Helsinki (NO.2024.283). Implicit consent was obtained from all patients at the time of submission of the questionnaire.

Data and code availability

Data will be made available on request.

Declaration of competing interest

The authors declare that the research was conducted in the absence of any commercial or financial relationships that could be construed as a potential conflict of interest.

Acknowledgments

This research was supported by [the clinical medical research center project of Jiangxi Province] under grant(s) [Grant No. 20223BCG74001].

References

[1] D. Steel, Retinal detachment, Clin. Evid. 2014 (2014).
[2] J.Y. Ge, Z.L. Teo, M.L. Chee, Y.-C. Tham, T.H. Rim, C.-Y. Cheng, , et al.N. Cheung, International incidence and temporal trends for rhegmatogenous retinal detachment: a systematic review and meta-analysis, Surv. Ophthalmol. (2023), https://doi.org/10.1016/j.survophthal.2023.11.005.
[3] R. Anguita, J. Roth, A. Makuloluwa, S. Shahid, M. Katta, H. Khalid, , et al.D.G. Charteris, Late presentation of retinal detachment: clinical features and surgical outcomes, Retina 41 (2021) 1833–1838, https://doi.org/10.1097/IAE.0000000000003131.
[4] A. Ibanga, O.N. Okonkwo, W. Ovienria, I. Oyekunle, T. Akanbi, D. Nkanga, et al., Collaborative retinal research network study, the fellow eye of retinal detachment patients: vision and clinical presentation, Niger. J. Clin. Pract. 26 (2023) 1342–1347, https://doi.org/10.4103/njcp.njcp_101_23.
[5] T. Schick, H. Heimann, F. Schaub, [Retinal detachment Part 1 - epidemiology, risk factors, clinical characteristics, diagnostic approach], Klin Monbl Augenheilkd 237 (2020) 1479–1491, https://doi.org/10.1055/a-1243-1363.
[6] K. Dong, Z.C. Zhu, F.H. Wang, G.J. Ke, Z. Yu, X. Xu, Activation of autophagy in photoreceptor necroptosis after experimental retinal detachment, Int. J. Ophthalmol. 7 (2014) 745–752, https://doi.org/10.3980/j.issn.2222-3959.2014.05.01.
[7] J.A. Choi, Y.J. Kim, B.-R. Seo, J.-Y. Koh, Y.H. Yoon, Potential role of zinc dyshomeostasis in matrix metalloproteinase-2 and -9 activation and photoreceptor cell death in experimental retinal detachment, Investigative Opthalmology & Visual Science 59 (2018), https://doi.org/10.1167/iovs.17-23502.
[8] S. Vujosevic, M.M. Parra, M.E. Hartnett, L. O'Toole, A. Nuzzi, C. Limoli, , et al.P. Nucci, Optical coherence tomography as retinal imaging biomarker of neuroinflammation/neurodegeneration in systemic disorders in adults and children, Eye 37 (2022) 203–219, https://doi.org/10.1038/s41433-022-02056-9.
[9] S. Schnichels, F. Paquet-Durand, M. Löscher, T. Tsai, J. Hurst, S.C. Joachim, , et al.A. Klettner, Retina in a dish: cell cultures, retinal explants and animal models for common diseases of the retina, Prog. Retin. Eye Res. 81 (2021), https://doi.org/10.1016/j.preteyeres.2020.100880.
[10] Z.-Y. Zhang, Y.-J. Sun, J.-Y. Song, B. Fan, G.-Y. Li, Experimental models and examination methods of retinal detachment, Brain Res. Bull. 169 (2021) 51–62, https://doi.org/10.1016/j.brainresbull.2021.01.004.
[11] A. Ibrar, M. Panayiotis, E.A. Mohamed, Recognising and managing retinal detachments, Br. J. Hosp. Med. 82 (2021) 1–11, https://doi.org/10.12968/hmed.2021.0145.
[12] X. Huang, D. Li, H.-J. Li, Y.-L. Zhong, S. Freeberg, J. Bao, , et al.Y. Shao, Abnormal regional spontaneous neural activity in visual pathway in retinal detachment patients: a resting-state functional MRI study, Neuropsychiatric Dis. Treat. 13 (2017) 2849–2854, https://doi.org/10.2147/ndt.S147645.
[13] T. Su, Y.-Q. Shu, K.-C. Liu, L. Ye, L.-L. Chen, W.-Q. Shi, , et al.Y. Shao, Functional connectivity of paired default mode network subregions in retinal detachment, Translational Vision Science & Technology 7 (2018), https://doi.org/10.1167/tvst.7.6.15.
[14] H.-H. Kang, Y.-Q. Shu, L. Yang, P.-W. Zhu, D. Li, Q.-H. Li, , et al.Y. Shao, Measuring abnormal intrinsic brain activities in patients with retinal detachment using amplitude of low-frequency fluctuation: a resting-state fMRI study, Int. J. Neurosci. 129 (2019) 681–686, https://doi.org/10.1080/00207454.2018.1554657.
[15] Y. Shao, L. Yang, P.W. Zhu, T. Su, X.Z. Zhou, B. Li, , et al.Q. Zhou, Functional connectivity density alterations in middle-age retinal detachment patients, Brain and Behavior 11 (2021), https://doi.org/10.1002/brb3.1783.
[16] Y.-C. Yang, Q.-Y. Li, M.-J. Chen, L.-J. Zhang, M.-Y. Zhang, Y.-C. Pan, , et al.Y. Shao, Investigation of changes in retinal detachment-related brain region activities and functions using the percent amplitude of fluctuation method: a resting-state functional magnetic resonance imaging study, Neuropsychiatric Dis. Treat. 17 (2021) 251–260, https://doi.org/10.2147/ndt.S292132.
[17] Y. Ji, Y.-y. Wang, Q. Cheng, W.-w. Fu, S.-q. Huang, P.-p. Zhong, , et al.X.-r. Wu, Machine learning analysis reveals aberrant dynamic changes in amplitude of low-frequency fluctuations among patients with retinal detachment, Front. Neurosci. 17 (2023), https://doi.org/10.3389/fnins.2023.1227081.
[18] D.J. Watts, S.H. Strogatz, Collective dynamics of 'small-world' networks, Nature 393 (1998) 440–442, https://doi.org/10.1038/30918.
[19] E. Bullmore, O. Sporns, Complex brain networks: graph theoretical analysis of structural and functional systems, Nat. Rev. Neurosci. 10 (2009) 186–198, https://doi.org/10.1038/nrn2575.
[20] L. Kuang, Y. Gao, Z. Chen, J. Xing, F. Xiong, X. Han, White matter brain network research in alzheimer's disease using persistent features, Molecules 25 (2020), https://doi.org/10.3390/molecules25112472.
[21] S.-Y. Lin, C.-P. Lin, T.-J. Hsieh, C.-F. Lin, S.-H. Chen, Y.-P. Chao, , et al.L.-W. Kuo, Multiparametric graph theoretical analysis reveals altered structural and functional network topology in Alzheimer's disease, Neuroimage: Clinical 22 (2019), https://doi.org/10.1016/j.nicl.2019.101680.
[22] P. Finotelli, C.G. Forlim, L. Klock, A. Pini, J. Bächle, L. Stoll, , et al.S. Kühn, New graph-theoretical-multimodal approach using temporal and structural correlations reveals disruption in the thalamo-cortical network in patients with schizophrenia, Brain Connect. 9 (2019) 760–769, https://doi.org/10.1089/brain.2018.0654.
[23] Y. Cao, Y. Zhan, M. Du, G. Zhao, Z. Liu, F. Zhou, , et al.L. He, Disruption of human brain connectivity networks in patients with cervical spondylotic myelopathy, Quant. Imag. Med. Surg. 11 (2021) 3418–3430, https://doi.org/10.21037/qims-20-874.
[24] G. Zhao, Y. Zhan, J. Zha, Y. Cao, F. Zhou, L. He, Abnormal intrinsic brain functional network dynamics in patients with cervical spondylotic myelopathy, Cognitive Neurodynamics 17 (2022) 1201–1211, https://doi.org/10.1007/s11571-022-09807-0.
[25] D. Liu, J. Gao, T. You, S. Li, F. Cai, C. Pei, , et al.X. Zeng, Brain functional network analysis of patients with primary angle-closure glaucoma, Dis. Markers 2022 (2022) 2731007, https://doi.org/10.1155/2022/2731007.

[26] R.S. Nancy Noella, J. Priyadarshini, Machine learning algorithms for the diagnosis of Alzheimer and Parkinson disease, J. Med. Eng. Technol. 47 (2022) 35–43, https://doi.org/10.1080/03091902.2022.2097326.
[27] F.-F. Huang, X.-Y. Yang, J. Luo, X.-J. Yang, F.-Q. Meng, P.-C. Wang, , et al.Z.-J. Li, Functional and structural MRI based obsessive-compulsive disorder diagnosis using machine learning methods, BMC Psychiatr. 23 (2023), https://doi.org/10.1186/s12888-023-05299-2.
[28] C.-G. Yan, Y.-F. Zang, DPARSF: A MATLAB Toolbox for "Pipeline" Data Analysis of Resting-State fMRI, Front Syst Neurosci (2010), https://doi.org/10.3389/fnsys.2010.00013.
[29] W. Liao, G.-R. Wu, Q. Xu, G.-J. Ji, Z. Zhang, Y.-F. Zang, , et al.G. Lu, DynamicBC: a matlab toolbox for dynamic brain connectome analysis, Brain Connect. 4 (2014) 780–790, https://doi.org/10.1089/brain.2014.0253.
[30] A.I. Luppi, D. Golkowski, A. Ranft, R. Ilg, D. Jordan, D.K. Menon, , et al.E.A. Stamatakis, Brain network integration dynamics are associated with loss and recovery of consciousness induced by sevoflurane, Hum. Brain Mapp. 42 (2021) 2802–2822, https://doi.org/10.1002/hbm.25405.
[31] F.A. Espinoza, J. Liu, J. Ciarochi, J.A. Turner, V.M. Vergara, A. Caprihan, , et al.V.D. Calhoun, Dynamic functional network connectivity in Huntington's disease and its associations with motor and cognitive measures, Hum. Brain Mapp. 40 (2019) 1955–1968, https://doi.org/10.1002/hbm.24504.
[32] Q. Yu, E.B. Erhardt, J. Sui, Y. Du, H. He, D. Hjelm, , et al.V.D. Calhoun, Assessing dynamic brain graphs of time-varying connectivity in fMRI data: application to healthy controls and patients with schizophrenia, Neuroimage 107 (2015) 345–355, https://doi.org/10.1016/j.neuroimage.2014.12.020.
[33] M. Rubinov, O. Sporns, Complex network measures of brain connectivity: uses and interpretations, Neuroimage 52 (2010) 1059–1069, https://doi.org/10.1016/j.neuroimage.2009.10.003.
[34] J. Wang, X. Wang, M. Xia, X. Liao, A. Evans, Y. He, GRETNA: a graph theoretical network analysis toolbox for imaging connectomics, Front. Hum. Neurosci. 9 (2015) 386, https://doi.org/10.3389/fnhum.2015.00386.
[35] K.J. Friston, S. Achard, E. Bullmore, Efficiency and cost of economical brain functional networks, PLoS Comput. Biol. 3 (2007), https://doi.org/10.1371/journal.pcbi.0030017.
[36] S. Maslov, K. Sneppen, Specificity and stability in topology of protein networks, Science 296 (2002) 910–913, https://doi.org/10.1126/science.1065103.
[37] D. Lei, W.H.L. Pinaya, T. van Amelsvoort, M. Marcelis, G. Donohoe, D.O. Mothersill, , et al.A. Mechelli, Detecting schizophrenia at the level of the individual: relative diagnostic value of whole-brain images, connectome-wide functional connectivity and graph-based metrics, Psychol. Med. 50 (2019) 1852–1861, https://doi.org/10.1017/s0033291719001934.
[38] F. Dong, Z. Zhang, T. Chu, K. Che, Y. Li, Q. Gai, , et al.H. Xie, Altered dynamic amplitude of low-frequency fluctuations in patients with postpartum depression, Behav. Brain Res. 433 (2022), https://doi.org/10.1016/j.bbr.2022.113980.
[39] Z. Fu, Y. Tu, X. Di, Y. Du, G.D. Pearlson, J.A. Turner, , et al.V.D. Calhoun, Characterizing dynamic amplitude of low-frequency fluctuation and its relationship with dynamic functional connectivity: an application to schizophrenia, Neuroimage 180 (2018) 619–631, https://doi.org/10.1016/j.neuroimage.2017.09.035.
[40] L. Zhao, D. Wang, S.W. Xue, Z. Tan, Y. Wang, Z. Lian, Aberrant state-related dynamic amplitude of low-frequency fluctuations of the emotion network in major depressive disorder, J. Psychiatr. Res. 133 (2021) 23–31, https://doi.org/10.1016/j.jpsychires.2020.12.003.
[41] Y. Wang, L. Chen, F. Cai, J. Gao, F. Ouyang, Y. Chen, , et al.X. Zeng, Altered functional connectivity of the thalamus in primary angle-closure glaucoma patients: a resting-state fMRI study, Front. Neurol. 13 (2022), https://doi.org/10.3389/fneur.2022.1015758.
[42] P. Coppola, L.R.B. Spindler, A.I. Luppi, R. Adapa, L. Naci, J. Allanson, , et al.E.A. Stamatakis, Network dynamics scale with levels of awareness, Neuroimage 254 (2022) 119128, https://doi.org/10.1016/j.neuroimage.2022.119128.
[43] S. Lin, P. Wu, S. Duan, Q. Du, S. Guo, Z. Chen, , et al.H. Zhao, Altered functional brain networks in coronary heart disease: independent component analysis and graph theoretical analysis, Brain Struct. Funct. (2023), https://doi.org/10.1007/s00429-023-02724-w.
[44] J. Li, Y. Shu, L. Chen, B. Wang, L. Chen, J. Zhan, , et al.X. Zeng, Disrupted topological organization of functional brain networks in traumatic axonal injury, Brain Imaging Behav (2023), https://doi.org/10.1007/s11682-023-00832-z.
[45] K. Song, J. Li, Y. Zhu, F. Ren, L. Cao, Z.G. Huang, Altered small-world functional network topology in patients with optic neuritis: a resting-state fMRI study, Dis. Markers 2021 (2021) 9948751, https://doi.org/10.1155/2021/9948751.
[46] C.Y. Wee, Z. Zhao, P.T. Yap, G. Wu, F. Shi, T. Price, , et al.D. Shen, Disrupted brain functional network in internet addiction disorder: a resting-state functional magnetic resonance imaging study, PLoS One 9 (2014) e107306, https://doi.org/10.1371/journal.pone.0107306.
[47] X. Yang, J. Liu, Y. Meng, M. Xia, Z. Cui, X. Wu, , et al.Y. He, Network analysis reveals disrupted functional brain circuitry in drug-naive social anxiety disorder, Neuroimage 190 (2019) 213–223, https://doi.org/10.1016/j.neuroimage.2017.12.011.
[48] V. Latora, M. Marchiori, Efficient behavior of small-world networks, Phys. Rev. Lett. 87 (2001) 198701, https://doi.org/10.1103/PhysRevLett.87.198701.
[49] J.R. Cohen, The behavioral and cognitive relevance of time-varying, dynamic changes in functional connectivity, Neuroimage 180 (2018) 515–525, https://doi.org/10.1016/j.neuroimage.2017.09.036.
[50] X. Liao, M. Cao, M. Xia, Y. He, Individual differences and time-varying features of modular brain architecture, Neuroimage 152 (2017) 94–107, https://doi.org/10.1016/j.neuroimage.2017.02.066.
[51] C.G. Yan, R.C. Craddock, Y. He, M.P. Milham, Addressing head motion dependencies for small-world topologies in functional connectomics, Front. Hum. Neurosci. 7 (2013) 910, https://doi.org/10.3389/fnhum.2013.00910.
[52] Y. Zou, W. Tang, X. Qiao, J. Li, Aberrant modulations of static functional connectivity and dynamic functional network connectivity in chronic migraine, Quant Imaging Med Surg 11 (2021) 2253–2264, https://doi.org/10.21037/qims-20-588.
[53] L. Steiner, A. Federspiel, N. Slavova, R. Wiest, S. Grunt, M. Steinlin, , et al.R. Everts, Functional topography of the thalamo-cortical system during development and its relation to cognition, Neuroimage 223 (2020) 117361, https://doi.org/10.1016/j.neuroimage.2020.117361.
[54] K. Wang, T. Jiang, C. Yu, L. Tian, J. Li, Y. Liu, , et al.K. Li, Spontaneous activity associated with primary visual cortex: a resting-state FMRI study, Cereb Cortex 18 (2008) 697–704, https://doi.org/10.1093/cercor/bhm105.
[55] D.L. Ringach, M.J. Hawken, R. Shapley, Binocular eye movements caused by the perception of three-dimensional structure from motion, Vision Res 36 (1996) 1479–1492, https://doi.org/10.1016/0042-6989(95)00285-5.
[56] S. Rosemann, J.P. Rauschecker, Disruptions of default mode network and precuneus connectivity associated with cognitive dysfunctions in tinnitus, Sci. Rep. 13 (2023) 5746, https://doi.org/10.1038/s41598-023-32599-0.
[57] J. Wu, S. Kang, J. Su, K. Liu, L. Fan, X. Ma, , et al.D. Hu, Altered functional network connectivity of precuneus and executive control networks in type 2 Diabetes Mellitus without cognitive impairment, Front. Neurosci. 16 (2022) 887713, https://doi.org/10.3389/fnins.2022.887713.
[58] Y. Shu, Y. Huang, J. Chen, L. Chen, G. Cai, Y. Guo, , et al.X. Zeng, Effects of primary angle-closure glaucoma on interhemispheric functional connectivity, Front. Neurosci. 17 (2023) 1053114, https://doi.org/10.3389/fnins.2023.1053114.
[59] P.K. Gupta, J.P. Berdahl, C.C. Chan, K.M. Rocha, E. Yeu, B. Ayres, , et al.A.C.C.C. from the, The corneal endothelium: clinical review of endothelial cell health and function, J. Cataract Refract. Surg. 47 (2021) 1218–1226, https://doi.org/10.1097/j.jcrs.0000000000000650.